Journal of CO2 Utilization 83 (2024) 102771

Contents lists available at ScienceDirect

Journal of CO2 Utilization

journal homepage: www.elsevier.com/locate/jcou

Poly(ionic liquid)-based aerogels for continuous-flow CO_2 upcycling

Raquel V. Barrulas [a,1], Cristopher Tinajero [b,2], Diogo P.N. Ferreira [a], Carlos Illanes-Bordomás [d,3], Victor Sans [b,4], Manuela Ribeiro Carrott [c,5], Carlos A. García-González [d,6], Marcileia Zanatta [b,*,7], Marta C. Corvo [a,*,8]

[a] i3N|Cenimat, Department of Materials Science (DCM), NOVA School of Science and Technology, NOVA University of Lisbon, Caparica 2829-516, Portugal
[b] Institute of Advanced Materials (INAM), Universitat Jaume I, Avda Sos Baynat s/n, Castellón 12071, Spain
[c] LAQV-REQUIMTE, Institute for Research and Advanced Studies, Department of Chemistry and Biochemistry, School of Sciences and Technology, University of Évora, Évora 7000-671, Portugal
[d] AerogelsLab, Department of Pharmacology, Pharmacy and Pharmaceutical Technology, I+D Farma Group (GI-1645), Faculty of Pharmacy, iMATUS and Health Research Institute of Santiago de Compostela (IDIS), Universidade de Santiago de Compostela, Santiago de Compostela E-15782, Spain

ARTICLE INFO

Keywords:
Polymeric ionic liquids
Aerogel
Porous materials
CO_2 cycloadditions
Packed-bed reactors

ABSTRACT

The atmospheric concentration of CO_2 is rising at an alarming pace, creating a pressing need for new and sustainable materials capable of capture and conversion. Poly(ionic liquid)s (PILs) are particularly effective catalysts for processes at or near atmospheric pressure. PILs industrial application poses challenges due to the low porosity of PIL, the limited batch conversion capacity, and the difficulties in reuse. To overcome these limitations, we herein propose the use of *AEROPILs* catalysts obtained from the integration of PILs in chitosan-based aerogels. These cost-effective highly porous materials have unique and tuneable porous properties making them not only ideal sustainable CO_2 sorbents but also promising heterogeneous catalysts. While *AEROPILs* show moderate yields for CO_2 conversion in batch mode, high catalytic activity was achieved when *AEROPILs* were used to catalyse the CO_2 cycloaddition reaction to epoxides in packed-bed reactors operated under continuous flow. The catalytic activity and stability were maintained over 60 h without activity loss, and high productivity (space-time yield of 21.18 $g_{prod}\ h^{-1}\ L^{-1}$). This research reveals the pioneering use of *AEROPILs* to efficiently upcycle CO_2 into cyclic carbonate under a continuous flow setup.

1. Introduction

Global warming demands the globalisation of CO_2 capture and utilisation (CCU) technologies [1]. The use of CO_2 as a C1 building block for synthesising alternative chemical products, such as cyclic carbonates, using epoxides is regarded as an environmentally sound and proficient strategy. Cyclic carbonates can be used as polymer precursors, aprotic polar solvents, fuel additives, or electrolytes in batteries [2–6]. In recent times, there has been a notable emergence of poly(ionic liquid)s (PILs), which combine the attributes of ionic liquids (ILs) and the features of polymers. ILs are salts encompassing organic cations conjoined with organic or inorganic anions, with melting points below 100 °C. PILs feature a substantial macromolecular architecture that imparts augmented mechanical robustness, heightened manipulability in processes, increased durability, and precise governance of meso to nanostructural attributes. The elevated processability exhibited by these compounds holds pertinence in industrial domains encompassing electrochemistry, analytical chemistry, biosciences, catalysis, sensors,

* Corresponding authors.
E-mail addresses: zanatta@uji.es (M. Zanatta), marta.corvo@fct.unl.pt (M.C. Corvo).
[1] ORCID ID: 0000-0001-5225-8714
[2] ORCID ID: 0000-0002-8093-5863
[3] ORCID ID: 0000-0001-7001-588X
[4] ORCID ID: 0000-0001-7045-5244
[5] ORCID ID: 0000-0003-4856-5150
[6] ORCID ID: 0000-0001-9542-3679
[7] ORCID ID: 0000-0002-3080-3627
[8] ORCID ID: 0000-0003-0890-6133

https://doi.org/10.1016/j.jcou.2024.102771
Received 16 February 2024; Received in revised form 2 April 2024; Accepted 16 April 2024

magnetism, energy conversion, and environmental applications [7–10]. PILs have been found to increase CO_2 sorption capacity, but materials with tailored porosity remain a significant challenge. Therefore, porous PILs emerged as promising materials for CO_2 capture (CC) and catalysis due to their high surface area, tuneable pore size, and selective functional groups [11–17]. The development of porous substrates derived from PILs has predominantly revolved around ionic porous organic polymers (IPOPs) and, more contemporarily, molecularly imprinted polymers and aerogels. This progression has generated the formulation of innovative substances merging PILs with porosity, thereby enhancing efficacy and selectivity. Recent advances in developing porous PILs highlight their potential for addressing environmental and energy-related challenges [18–22].

Solid catalysts can be easily applied in fixed-bed reactors, continuous flow systems, or others suitable for large-scale processes [2,23]. In contrast to batch processes, continuous flow catalytic systems offer several advantages. They favour mixing, handle heat transfer more effectively, optimise catalytic performance by enhancing phase interactions, and boost productivity through continuous reagent feeding and product removal from the reactor. Overall, they offer a more reliable, scalable, secure, and efficient approach for conducting chemical reactions, making them a highly appealing technology for industrial applications [24–28].

In previous works, Iglesias *et al.* [6] and Valverde *et al.* [28] reported cycloadditions of CO_2 to produce cyclic carbonates using 3D printed reactors and ILs in continuous flow. However, the reported reactors lack porosity, and catalysis only occurs on the surface of the material. In the present work, *AEROPILs* were optimized to catalyse CO_2 not only at the surface but also on the core, exhibiting an increased catalytic load with high stability. Chitosan-based aerogels were envisioned to achieve this.

Aerogels are lightweight nanostructured materials with high porosity and specific surface area. Silica aerogels are already being used for CC [29,30]. However, formulating aerogels from biopolymers such as chitosan is advantageous as it has basic nitrogen groups that can enhance the interactions with acidic CO_2 [31]. Besides being biodegradable, chitosan has the advantage of using biomass residue from processed seafood products as a starting material, increasing profitability by recycling waste [32–34]. Chitosan aerogels and their composites are innovative and eco-friendly materials characterized by significant porosity, extensive specific surface area, excellent biodegradability, biocompatibility, and widespread availability. The synthesis of chitosan aerogels takes advantage of the polymer's functional groups to improve physicochemical properties, usually through colloidal formation from molecular precursors, or the use of particle-based precursors. Both methods impact the aerogel's properties and factors such as precursor concentration, crosslinkers, and drying procedures play crucial roles, which are vital for applications ranging from catalysis to wastewater treatment [22]. The amine groups in chitosan's structure contribute to its versatility, allowing for functionalization through graft reactions and ionic interactions due to their basic nature. While surface area and porosity are crucial for CO_2 capture and fixation, chitosan itself has a limited surface area and a crystalline structure. Therefore, chitosan composites with porous materials having high specific surface area enhance the effectiveness in CO_2 capture and fixation. This is supported by research indicating that the abundant amine groups in chitosan facilitate the adsorption of CO_2 molecules, but its lower surface area limits the adsorption capacity [35,36].

Previously, we described for the first time a simple and economically viable methodology for producing *AEROPILs* (composite aerogel beads with PILs and chitosan), and tested them for CC [37]. Here, we report, for the first time, the use of *AEROPILs* (Fig. 1) in continuous flow packed-bed reactors in an automatised flow platform that enabled the fast screening of different conditions. *AEROPILs* produced a highly efficient catalytic system for CO_2 cycloadditions to epoxides, moving a step closer to industrial applications.

2. Materials and methods

2.1. Material

Chitosan (deacetylation degree 75–85 %, viscosity 20–300 mPa.s, Mw 50–190 kDa), glutaraldehyde solution (grade II, 25 wt % in H_2O), 1-vinylimidazole (≥99 % purity), 4-vinylbenzyl chloride (90 % purity), 2-bromoethylamine hydrobromide (99 % purity), poly(diallyldimethylammonium) chloride (**P2**) solution (20 wt % in H_2O, viscosity 250–500 mPa.s, average Mw 100–200 kDa), triethylamine (≥99.5 % purity), tributylphosphine (≥93.5 % purity), styrene oxide (97 % purity) and epichlorohydrin (≥99 % purity) were supplied by Sigma-Aldrich (St. Louis, MO, USA). Ethylene glycol diglycidyl ether (EGDE) mixture and 1,2-butylene oxide (99 % purity) were acquired

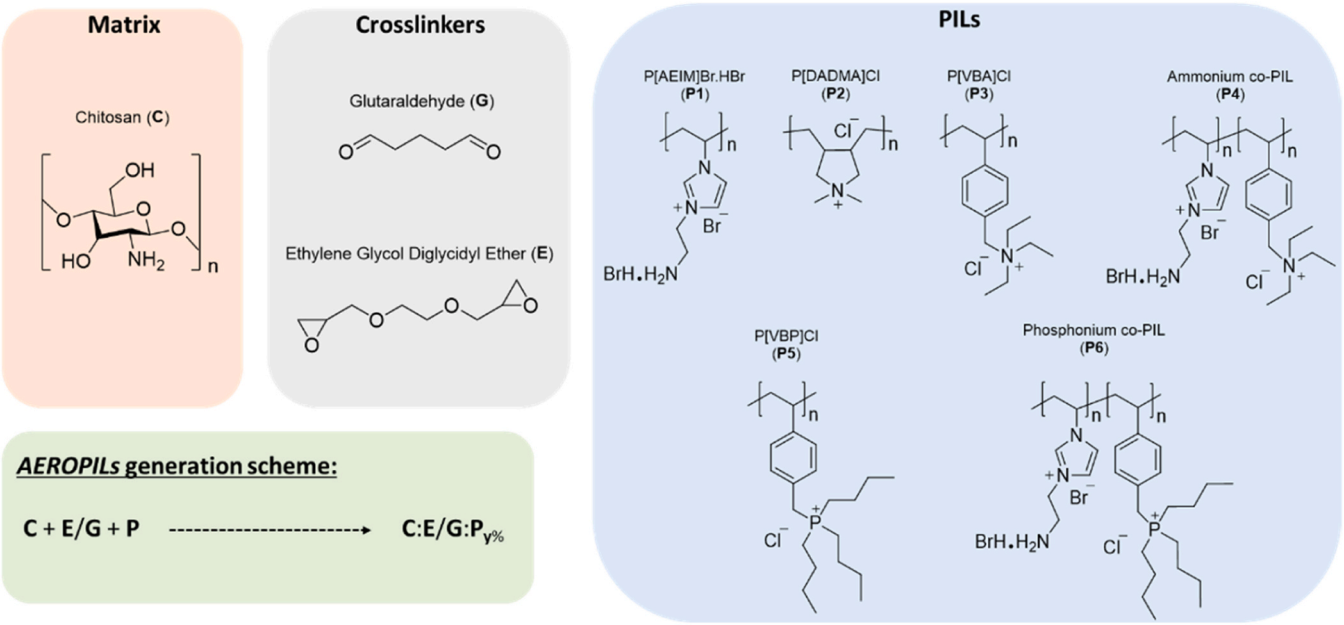

Fig. 1. Chemical structures of the matrix (C), crosslinkers (E or G) and PILs (P) in *AEROPILs* formulations.

from TCI Chemicals (Tokyo, JP). 2,2'-Azobis(2-methylpropionitrile) (AIBN) was acquired from Glentham Life Sciences (Corsham, UK). Glacial acetic acid, isopropanol (IPA), and absolute ethanol (EtOH) were acquired from VWR (Radnor, PA, USA). NaOH (98 % purity) was acquired from Panreac (Barcelona, Spain). DMSO-d_6 and $CDCl_3$ were acquired from Euriso-top (Saint-Aubin, France). Water was purified using reverse osmosis (resistivity > 18 MΩ.cm, Milli-Q, Millipore®, Madrid, Spain). Carbon dioxide (99.8 % purity) was supplied by Nippon Gases (Madrid, Spain). Carbon dioxide (99.998 % purity) supplied by Air Liquid was used in the catalytic reactions. He 4.6 and CO_2 4.5, supplied by Linde Portugal, were used in the thermogravimetric analysis (TGA) and CO_2 capture experiments. All chemicals were used without further purification.

2.2. IL and PIL synthesis

ILs *p*-vinylbenzyltriethylammonium chloride ([VBA]Cl), *p*-vinylbenzyltributylphosphonium chloride ([VBP]Cl) and 1-aminoethylimidazolium bromide hydrobromide ([AEIM]Br.HBr) were synthesised and characterised as outlined in Section 1 (Figure S.1) and Section 4 of the Supporting Information. PILs poly(1-aminoethylimidazolium bromide hydrobromide) (**P1**), poly(*p*-vinylbenzyltriethylammonium) chloride (**P3**), poly(*p*-vinylbenzyltributylphosphonium) chloride (**P5**) and copolymer$_{50/50}$ poly(*p*-vinylbenzyltriethylammonium chloride-co-aminoethylimidazolium bromide hydrobromide) (**P4**) and copolymer$_{50/50}$ poly(*p*-vinylbenzyltributylphosphonium chloride-co-aminoethylimidazolium bromide hydrobromide) (**P6**) were synthesised and characterised as outlined in Section 2 (Figure S.2) and Section 4 of the Supporting Information.

2.3. Chitosan aerogel beads formulation

2.3.1. Chitosan hydrogels formulation

Hydrogel particles were synthesised using the sol-gel approach, following the methodology delineated in López-Iglesias *et al.*[32] and Barrulas *et al.*[37]. Initially, a 2.5 % w/v chitosan solution was prepared by dissolving chitosan in Milli-Q water with a 1 % (v/v) acetic acid content, resulting in a 30 mL solution volume. The mixture underwent mechanical agitation for 8 h, after which it was allowed to settle until the cessation of gas bubble formation occurred during the stirring process.

Chitosan (C) solutions were then prepared with several crosslinkers. The addition of either glutaraldehyde (G) or EGDE (E) was evaluated, as well as the use of heating after the crosslinker addition (50 °C). Glutaraldehyde was added at a concentration previously reported in the literature – 0.30 % w/w (glutaraldehyde/chitosan) to avoid leakage of the PILs [37]. Chitosan solutions with different loadings of PILs: **P1**, **P2**, **P3**, and **P4** (30 %, 50 % and 80 % w/w with respect to chitosan), and glutaraldehyde (0.30 %) were used to produce beads. Also, chitosan solutions with different loadings of **P4**, **P5**, **P6**, and **P2** (50 % and 80 % w/w with respect to chitosan) and with EGDE 32 % w/w (EGDE/chitosan) directly incorporated were used to produce beads. The solutions were then stirred for 15 min at 50 °C according to the procedure described by Martucci et al. [38] to activate the crosslinker. Chitosan solutions with different loadings of PILs **P1**, **P2** and **P4** (30 % w/w with respect to chitosan) and without crosslinker directly incorporated were also used to produce beads. In all instances, PILs were previously solubilised within a 3 mL aqueous volume, which was subsequently subtracted from the overall water volume employed in the chitosan solution formulation. Following this, aliquots of the resultant chitosan solution (ranging from 15 to 18 mL) were incrementally introduced via a plastic syringe (with a nozzle diameter of 2 mm) into a 100 mL gelation bath containing 1 mol L^{-1} NaOH. The infusion was maintained at a constant flow rate of 0.65 mL min^{-1}, facilitated by a syringe pump (AL-1000, World Precision Instruments, Sarasota, FL, USA). The vertical distance from the syringe to the bath's surface was approximately 16.5 cm. The droplets solidified upon contact with the NaOH solution, producing hydrogel beads. The time between the addition of the crosslinker and the prilling process to prepare the beads in the NaOH solution was approximately 15 min. These beads were retained within the gelation bath for either 24 h without subsequent treatment or for 2 h when subsequent steps of crosslinking or heating were administered. So, after gelation, some sample variations were subjected to heating with a water bath (blanks) or with an aqueous EGDE solution (ratio 1:1 EGDE:NH_2) at 50 °C for 3 h, according to procedures described in the literature [39–41]. The complete table with the prepared *AEROPILs* is outlined in Section 6 (Tables S.2 and S.3) of the Supporting Information.

2.3.2. Solvent exchange

The gel beads were gently decanted from the beaker containing the gelation bath and promptly supplanted with 100 mL of absolute EtOH. Following a duration of 4 h, a subsequent solvent substitution was enacted utilising a comparable volume of EtOH to eliminate residual water content from the gel matrices.

2.3.3. Supercritical extraction of the gel solvent

The alcogel particles were inserted into Whatman paper cartridges and subsequently introduced either into the 400 mL autoclave module of the supercritical drying apparatus from Eurotechnica GmbH, Bargteheide, Germany or into the 300 mL autoclave module of a costume-made equipment from Paralab, Valbom, Portugal (Figure S.12). Previously, 100 mL of EtOH were introduced into the chamber, ensuring the prevention of premature EtOH evaporation from the alcogels before the achievement of supercritical conditions within the CO_2-EtOH mixture [32,42]. A continuous flow of $scCO_2$ at a rate of 15 g min^{-1} was directed through the autoclave housing the gels, which were maintained at an operational temperature of 40 °C and a pressure of 120 bar for a duration of 3.5 h.

Herein, *AEROPILs* samples are addressed as in the general symbology: **C:G:Mx:P$_{y\%}$** (where x is the methodology used for extra processing procedures and y is the percentage of PIL added with respect to chitosan); the terms **M1** (methodology associated with the crosslinker EGDE, represented as E, directly incorporated), **M2** (E incorporated into the aqueous bath), **M3** (aqueous bath subjected to heat) or **M4** (E incorporated into the aqueous bath subjected to heat) also appear related to extra processing procedures.

A compilation of the *AEROPILs* abbreviations in use throughout the manuscript is presented in Table 1.

Table 1
List of abbreviations.

Abbreviations	Meaning
C	Chitosan
E and EGDE	Ethylene glycol diglycidyl ether
G	Glutaraldehyde
Mx	Methodology for extra processing, where x = 1, 2, 3, or 4
M1	Methodology associated with the crosslinker EGDE directly incorporated
M2	Methodology with EGDE incorporated into the aqueous bath
M3	Methodology with aqueous bath subjected to heat
M4	Methodology with EGDE incorporated into the aqueous bath subjected to heat
P	PIL
$P_{y\%}$	y% w/w with respect to chitosan
P1	Poly(1-aminoethylimidazolium bromide hydrobromide)
P2	Poly(diallyldimethylammonium) chloride
P3	Poly(*p*-vinylbenzyltriethylammonium) chloride
P4	Copolymer$_{50/50}$ poly(*p*-vinylbenzyltriethylammonium chloride-co-aminoethylimidazolium bromide hydrobromide)
P5	Poly(*p*-vinylbenzyltributylphosphonium) chloride
P6	Copolymer$_{50/50}$ poly(*p*-vinylbenzyltributylphosphonium chloride-co-aminoethylimidazolium bromide hydrobromide)

2.4. Batch catalytic cycloaddition of CO_2 to epoxides

***AEROPILs* – Reaction conditions.** In a typical experiment, the epoxide substrate (1.4 mmol, 100 mg - 1st condition – or 829 mg to 1382 mg depending on the substrate, 11.5 mmol - 2nd condition) and the *AEROPIL* (100 mg) was added in a stainless-steel reactor (45 mL), which was flushed with CO_2 for three times before stirring under the appointed CO_2 atmosphere (10 bar). The reaction mixture was stirred under a CO_2 atmosphere at 135 °C for 72 h. The yield was determined by the ^{1}H NMR data (Section 8.2 of the Supporting Information).

2.5. Continuous flow catalytic cycloaddition of CO_2 to epoxides

In a typical catalytic reaction, the reaction mixture consisted of a solution of 1 M of epichlorohydrin in IPA. The reaction was conducted using a Vapourtec flow system, which comprised several key components: the 'R-4 Flow Reactor Heater' module, the 'R2S Pumping Module' equipped with two peristaltic pumps, and the 'R2C Pumping Module' featuring two HPLC type pumps. Additionally, the system was connected to an autosampler to facilitate automated sample collection. All these modules and systems were remotely controlled via a UA-OPC communication protocol, utilizing software developed in Python for this purpose. This mixture was pumped at 0.05 mL min^{-1} using an HPLC pump. Simultaneously, CO_2 was pumped at a nominal flow rate of 0.20 mL min^{-1} and mixed with the liquid phase using a T-mixer. The actual CO_2 flow rate was determined to be 41 μL min^{-1}, considering factors such as gas compression and solubility calculations in the solvent at a temperature of 25 °C. The CO_2 was directly pumped into a back pressure regulator operating at a nominal flow rate of 0.20 mL min^{-1}. This regulator aimed to maintain a constant gas flow into the T-mixer, ensuring a consistent pressure line for the gas-liquid mixture. The experimental flow rate of CO_2 was determined to be 41 μL min^{-1} by calculating the difference between the total flow rate (of the gas-liquid mixture) and the flow rate of the incompressible liquid in a known tubing volume and selected time. Considering the system's pressure conditions, this calculation yielded the actual CO_2 inlet flow rate. The reaction was conducted within a packed bed reactor containing the catalysts with **C:E:M1:P2$_{80\%}$**, **C:E:M1:P5$_{50\%}$**, **C:E:M1:P6$_{50\%}$**, **C:G:P4$_{30\%}$** and the control aerogel, operating at 120 °C and 6 bar pressure, with a residence time ranging from 98 to 104 min. The conversion and selectivity of CO_2 cycloaddition reactions were calculated by ^{1}H NMR spectra (using styrene as an internal standard). Residence time (RT) was calculated using Eq. 1:

$$Residence \quad time \quad (RT) = \frac{Vr(mL)}{Q\left(\frac{mL}{\min}\right)} \tag{1}$$

Where Vr represents the volume of the reactor according to different catalysts (**C:E:M1:P2$_{80\%}$** = 7.78 mL; **C:E:M1:P5$_{50\%}$** = 7.61 mL; **C:E:M1:P6$_{50\%}$** = 7.84 mL; **C:G:P4$_{30\%}$** = 8.04 mL; **P0** control = 7.95 mL), and Q is the flow rate obtained by adding the experimentally determined gas flow rate to the liquid flow rate. Productivity was determined to understand the applicability of these catalysts at an industrial level by considering the space-time yield (STY) using Eq. 2:

$$STY = \frac{product \quad weight}{volume \quad reactor \quad x \quad residence \quad time} = \frac{gprod}{L.h} \tag{2}$$

3. Results and Discussion

3.1. Morphological and textural properties of the chitosan aerogels

A library of stable chitosan aerogels with different PILs (**P1**, **P2**, **P3**, **P4**, **P5** and **P6**) was obtained. The presence of crosslinker and heating during the preparation were also assessed, being the general approach of the *AEROPILs* preparation procedure depicted in Figure S.13. Also, the respective physicochemical (Table S.2) and textural properties (Table S.3) are presented in Section 6 of Supporting Information. The overall porosity exhibited a notable elevation, surpassing 88.1 % for all cases. Being that the lowest overall porosities were observed in the cases where the direct incorporation of EGDE occurred within the chitosan solution (Table S.2, entries 6, 8 and 11). The crosslinking reaction with EGDE can be achieved by reacting the epoxide groups in the crosslinker with the amino groups (–NH_2) on the chitosan backbone and PIL [43–45]. In this case, with the increased percentage of crosslinker and PIL, the structure of the aerogel's fibres became denser and therefore, the overall porosity diminished. Relatively to the specific surface area, it has generally increased with a higher amount of **P4** and/or the use of EGDE directly in the chitosan solution, being a_{BET} values in the 173–748 m^2 g^{-1} range (Table S.3).

Through the characterisation by ATR-FTIR spectroscopy, it is possible to infer that when glutaraldehyde was used, **P4** was successfully incorporated into the aerogel beads (Fig. 2 **(A)**). The sample without **P4** exhibited differences in the regions at 1615 cm^{-1} (aromatic), 1328 cm^{-1} (N-containing aromatic ring), 831 cm^{-1} (C═C) and 697 cm^{-1} (aromatic). Also, the vibration band at 1750 cm^{-1} corresponding to the C═O carbonyl group of free glutaraldehyde was absent [37,46]. Analysing the differences arising from the crosslinkers, more PIL was incorporated in the structure when glutaraldehyde is added. When **P4** was used, the same trend was obtained, as this PIL contains terminal -NH_2 groups that can be crosslinkable with chitosan. The main differences were observed in the following regions: 1658 (-NH stretching vibration), 1584 (C═N bond formed between the amine residues of chitosan and the aldehyde terminals of the glutaraldehyde, adding to the amide II vibration from chitosan), 1476 (characteristic vibration of imidazolium N heterocycle cation), 1337 (-CH_3 deformation), 1024 (C-N bend), 831 (C═C) and 688 cm^{-1} (aromatic) [37,41,46,47].

Regarding the use of heating during the bead's preparation, there are no significant differences in the FTIR spectra (Figure S.4), which can be indicative of the hydrophilic PIL **P2** lixiviation when the beads are in the aqueous solution of the crosslinker EGDE. Therefore, this analysis shows no apparent advantage in using this heating step.

^{13}C CP-TOSS NMR spectra (Fig. 2 **(B)**) confirmed **P4** incorporation in the structure when glutaraldehyde was used with the chemical shifts that appear at 10 ppm, 43 ppm and between 120 and 142 ppm. The same was verified for **P2**, as shown in Figure S.11.

Samples were analysed using Raman confocal microscopy to determine the extent of the modification with PILs. This technique allows the mapping of the composition of the polymer with a penetration depth of approximately 10 μm. Fig. 2 **(C)** depicts the mapping obtained for the *AEROPIL* **C:G:P4$_{30\%}$** using different penetrations for the incident laser light. The analysis clarified that the PIL **P4** is present both at the surface and the interior of the bead, with apparently a higher amount at the surface. The mapping shows two different components, one in red corresponding to the chitosan and one in blue corresponding to a crystalline component compatible with the PIL. The blue region above the red line corresponds to air, the red region corresponds to the bead modification with **P4**, and the blue region below the red line corresponds to the interior of the bead, which is inaccessible to the analysis. Additionally, the Raman spectra of the different components can be observed on the right side of Fig. 2 **(C)**. The Raman spectrum of a bead with chitosan only reveals the presence of bands in the range of 2813–3000 cm^{-1} (-CH stretching), 1365 cm^{-1} and 1109 cm^{-1} (polysaccharide backbones), which is in accordance with the literature [48–50]. The analysis of the spectra of the interior and surface of the *AEROPIL* bead reveals new peaks assignable to imidazolium in the 1517–1384 cm^{-1} region where the C═C and C═N bond stretching bands of imidazolium appear [28]. There are also other bands at 3294 cm^{-1} (typically associated with -OH stretching vibration), 2192 cm^{-1} and 1911 cm^{-1} (often assigned to C═C stretching vibration of aromatic rings, such as those found in benzene derivatives). These results are consistent with the other characterisations that could help explain the possible CO_2 capture and

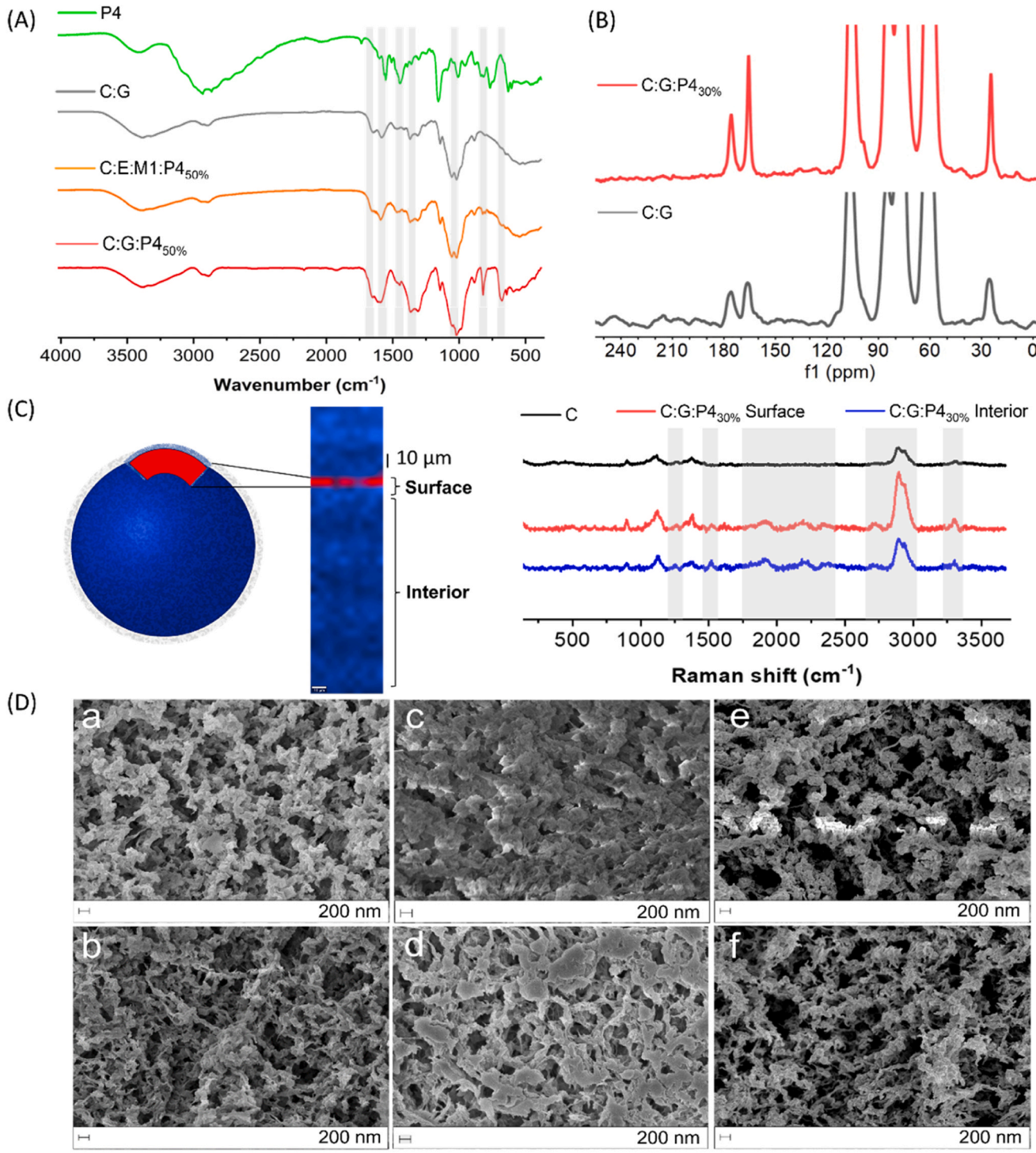

Fig. 2. **(A)** ATR-IR spectra of **P4** (green), **C:G** (grey), **C:E:M1:P4$_{50\%}$** (orange) and **C:G:P4$_{50\%}$** (red). **(B)** ^{13}C CP-TOSS NMR spectra of **C:G:P4$_{30\%}$** beads (red) and **C:G** (grey). **(C)** (Left) Schematic representation of the area of the bead **C:G:P4$_{30\%}$** observed and the corresponding mapping for the outer 10 µm depth of the bead. The blue region above the red line represents air, the red region represents the bead modification with **P4**, and the blue region below the red line corresponds to the bead interior that is impossible to see. (Right) Raman spectra correspond to the surface and interior of the *AEROPIL* bead compared to the C bead. **(D)** Textural appearance of the (a, c, e) surface of beads **C:G**, **C:G:P4$_{30\%}$**, **C:G:P1$_{30\%}$**, respectively, and (b, d, f) interior of beads **C:G**, **C:G:P4$_{30\%}$**, **C:G:P1$_{30\%}$**, respectively, by SEM imaging (scale bar: 200 nm).

catalytic activity since the active moiety for these PILs is effectively distributed into the final material.

The most promising beads were analysed through SEM microscopy. Fig. 2 (**D**) shows some images of *AEROPIL* beads from **P1** and **P4** with glutaraldehyde as a crosslinker, which presents high specific surface areas, especially when the amount of PIL is increased. Chitosan beads with the same amount of crosslinker are also provided for comparison. There is a dual porous structure in the inner and outer structure of the particles, as reported previously [37]. It is also possible to observe that according to the PIL identity, different changes were induced, both in the interior and surface of the beads. The beads with **P4** ((**D**) c and d) presented more structured fibres than those with **P1** ((**D**) e and f).

3.2. Batch catalytic activity of AEROPILs

The characterization of *AEROPILs*' efficacy towards CO_2 capture and the assessment of their affinity for this gaseous substrate, was done as elucidated by Barrulas *et al.*[37] and expounded upon in Section 7 of the Supporting Information. The CO_2 capture capacity (n_{CO2}) varies between 0.41 and 0.62 mmol g^{-1}, being **C:E:M1:P2$_{80\%}$** the best *AEROPIL* capturing CO_2. No direct correlation was observed between the *AEROPIL* porosity and CO_2 capture. Their performance is most likely a compromise of the textural and morphological properties and the respective PIL structure and dosage. The PIL addition percentage seems to be a determining factor since it can be observed in Figures S.14 and S.15 in Supporting Information that for the same PILs, increasing *y* enhances the CO_2 adsorption capacity. Afterwards, their catalytic activity was assessed in terms of conversion and selectivity.

To identify optimal candidates, a comprehensive screening process was conducted within batch reactions to advance their utilisation in continuous flow reactions, aligning with prospective industrial applications. The batch tested *AEROPILs* were selected for their textural and morphological properties, their ability to capture CO_2, and also to evaluate the performance of the different moieties that compose the PILs.

The outcome of these reactions was calculated by integrating the ^{1}H NMR signals in the spectrum of the crude mixture in $CDCl_3$. The results are summarised in Table 2.

As it is possible to verify, when PIL was present in the bead, there was a substantial enhancement in the catalytic activity compared to chitosan alone. However, although the conversion is high, there is a significative diol formation indicating the presence of water competing with the CO_2 reaction. The selectivity of the reaction for cyclic carbonates is relatively low in *AEROPILs* from **P1**, **P2** and **P3** (Table 2, entries 3–5, 9). Even, when considering a higher PIL content as in **C:E:M1:P2$_{80\%}$** (Table 2, entry 9), there is no further increase in the cyclic carbonate yield under this condition. Being that **P4** has crosslinkable moieties like **P1** but is less hydrophilic due to the presence of the vinylbenzyl derivative, the selectivity of **P4** was enhanced when highly crosslinked with EGDE (Table 2, entry 8). Therefore, a balance between the presence of crosslinkable moieties and the hydrophobicity of the PIL should be further pursued.

Due to suspicion of oligoether carbonates formation in *AEROPILs* from **P4** (Table 2, entry 7), GC-MS analysis of the reaction product was performed (Figure S.16), being the possible chemical structures of the additional products stated in Table S.4.

Alternative approaches were undertaken to enhance the selectivity for cyclic carbonates by increasing the substrate-to-catalyst ratio. This strategy aimed to facilitate the optimal impregnation of *AEROPILs* with the liquid substrate, thereby envisaging a substantial improvement in the reaction process. These innovative endeavours yielded favourable outcomes, specifically with butylene oxide and epichlorohydrin substrates, as demonstrated by the results outlined in Table 2, entries 10–13, 15. Styrene oxide (Table 2, entry 14) exhibits a lower conversion and selectivity, possibly due to being less reactive and bulkier. In the literature, several works neglect to provide data on selectivity (Table S.5). This level of scrutiny is significant, particularly when considering the prospective industrial implementation of these materials. Despite the present conversion occurring at 135 °C, the pressure is relatively low (10 bar). It is of relevance that reaction occurs in the absence of a co-catalyst and solvent and is also a metal-free catalytic reaction, which poses an environmental and economic advantage regarding some works in the literature [51–53]. Some good examples of using highly effective porous PILs as catalysts in CO_2 conversions have been reported [54,55], however, these materials are mainly described as powders.

The regenerative capability of the catalyst holds paramount significance, given its fundamental role in attaining a durable and sustainable material over an extended period. Consequently, within the boundaries of the present study, the utilisation of aerogel beads offers an additional reusability advantage, which has been refined through a progressively optimised protocol, as delineated in Section 8.3 of the Supporting Information. *AEROPIL* beads were completely rinsed with diethyl ether two consecutive times and subjected to moderate vacuum drying at 60 °C for at least 48 h until the next catalytic cycle under the same reaction conditions. Figure S.20 presents the CO_2 cycloaddition catalysed by *AEROPIL* **C:E:M1:P2$_{80\%}$** without co-catalyst and solvent. Five consecutive reactions were carried out at 135 °C and 10 bar of pressure for 72 h using approximately 10 wt % of catalyst (100 mg of catalyst and

Table 2
Batch CO_2 cycloaddition catalysed by *AEROPILs* in the absence of co-catalyst and solvent.

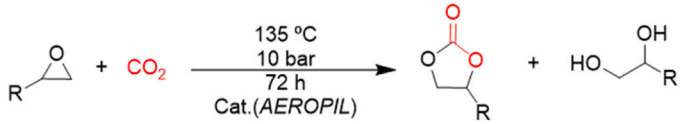

Entry	Catalyst	R	Catalyst amount (wt %)	Conversion (%)[b]	Selectivity (%)[b]
1	C	CH_2CH_3	100[c]	26	37
2	C:G	CH_2CH_3	100[c]	19	25
3	C:G:P3$_{30\%}$	CH_2CH_3	100[c]	92	11
4	C:G:P1$_{30\%}$	CH_2CH_3	100[c]	91	37
5	C:E:M2:P1$_{30\%}$	CH_2CH_3	100[c]	83	38
6	C:G:P4$_{30\%}$	CH_2CH_3	100[c]	94	44
7	C:G:P4$_{50\%}$	CH_2CH_3	100[c]	93	34[a]
8	C:E:M1:P4$_{50\%}$	CH_2CH_3	100[c]	74	75
9	C:E:M1:P2$_{80\%}$	CH_2CH_3	100[c]	98	22
10	C:E:M1:P2$_{80\%}$	CH_2CH_3	10[d]	59	80
11	C:E:M1:P5$_{50\%}$	CH_2CH_3	10[d]	22	80
12	C:E:M1:P6$_{50\%}$	CH_2CH_3	10[d]	32	81
13	C:G:P4$_{30\%}$	CH_2CH_3	10[d]	77	88
14	C:G:P4$_{30\%}$	Ph	10[d]	4	26
15	C:G:P4$_{30\%}$	CH_2Cl	10[d]	81	90

[a] Possible formation of oligoether carbonates detected.
[b] Conversion determined by integration of ^{1}H NMR signals of epoxide, diol, and cyclic carbonate on the reaction mixture with $CDCl_3$; selectivity for cyclic carbonates when diol is a by-product. The error of measurement is 6 %.
[c] 100 mg of catalyst, 100 mg (1.4 mmol) of epoxide.
[d] 100 mg of catalyst, 11.5 mmol (829 mg to 1382 mg) of epoxide.

11.5 mmol of butylene oxide). The catalyst was reused through the previously mentioned diethyl ether protocol between cycles. During these cycles, an increase in the conversion from the initial 59–72 % in the 3rd cycle and the selectivity enhancement from 80 % to 94 % led to the attempt to start the initial reaction with a similar diethyl ether pre-treatment. Indeed, when the 1st cycle started with pre-treated *AEROPIL*, the conversion enhanced from 59 % to 68 % and the selectivity from 80 % to 91 %. This could be due to the creation of new active sites with the washings and the vacuum drying. TGA thermograms (Section 4.4 in Supporting Information) show the presence of structural water that could be released with this treatment, enhancing the selectivity. Additionally, SEM and N_2 sorption results indicated that the morphology and porosity of *AEROPIL* **C:E:M1:P2$_{80\%}$** changed after catalysis. This might be due to residual cyclic carbonate trapped within the bead (Figure S.19), resulting in pore blockage. However, despite the loss of overall porosity, the average pore size increased (a_{BET} 30 ± 2 m^2 g^{-1}; $V_{P,BJH}$ 0.19 ± 0.01 cm^3 g^{-1}; $D_{P,BJH}$ 24.8 ± 1.2 nm – Table S.9, entry 1), the catalyst activity remained, and it was considered as a renewable and stable catalyst (Figure S.21). As observed for CO_2 capture, no direct correlation was found between the porosity and the catalytic activity of *AEROPILs* in these conditions.

Regardless of the reusability of the aerogel beads, they require washing processes with vacuum drying which entails energy and time costs. This makes the continuous flow catalysis even more advantageous as stated in the following section.

3.3. Continuous flow catalytic activity of AEROPILs

The catalysts that exhibited the best performance in batch were selected for the CO_2 cycloaddition experiments under continuous flow [6]. The following conditions were systematically optimised: temperature (80, 100 and 120 °C); CO_2 flow rate (0.10, 0.15 and 0.20 mL min^{-1}); liquid flow rate (0.05, 0.10, 0.15 and 0.20 mL min^{-1}); concentration variation of the epoxide (0.5, 1 and 2 M of epichlorohydrin in IPA); stability tests (liquid flow rate of 0.05 mL min^{-1}; CO_2 flow rate of 0.15 mL min^{-1}; 1 M of epichlorohydrin in IPA; 120 °C). First, the CO_2 flow rate and the liquid flow rate were fixed at 0.20 mL min^{-1} and 0.05 mL min^{-1} respectively and then the temperature was varied. With the temperature optimised and the liquid flow rate fixed at 0.05 mL min^{-1}, the CO_2 flow rate was then varied. The same principle was applied for the liquid flow rate and the concentration variation of the epoxide.

Optimisation efforts were undertaken using the **C:E:M1:P2$_{80\%}$** catalyst, while other catalysts, namely **C:E:M1:P5$_{50\%}$**, **C:E:M1:P6$_{50\%}$** and **C:G:P4$_{30\%}$**, were evaluated under the identified optimal reaction conditions. These *AEROPILs* were selected to understand the difference between ammonium and phosphonium, thus having different families of compounds. Additionally, a control aerogel (devoid of PIL) was tested for reference purposes, demonstrating a lack of catalytic activity.

The liquid phase, epichlorohydrin in IPA, was pumped with an HPLC pump into a T-mixer and mixed with CO_2 driven by a peristaltic pump. A back-pressure regulator (BPR) was added between the peristaltic pump and the T-mixer to ensure control over the gas flow rate (Fig. 3 (**A**)). The reaction mixture entered the reactor packed with the *AEROPILs* at a temperature of 120 °C (after optimisation), where the cycloaddition takes place. The BPR controlled the pressure of the reactor at 6 bar. After reaching a steady state, which was achieved in a time equivalent to three times the bed volume, the products were collected in triplicate vials using an automated fraction collector. The samples were analysed integrating the ^{1}H NMR signals in the spectrum of the reaction mixture in $CDCl_3$, using styrene as an internal standard. The results are herein presented in Fig. 3 (**B-E**).

According to the tests performed, the optimal reaction conditions were set at a temperature of 120 ºC, a liquid flow rate of 0.05 mL min^{-1} and a CO_2 flow rate of 0.15 mL min^{-1} (Figure S.22). When analysing Fig. 3 (**B**), it can be observed that the conversion decreases with increasing substrate concentration. The concentration of 1 M epichlorohydrin in IPA was selected. Although it presents an intermediate conversion, this concentration has a higher productivity, yielding sufficient sample as required for NMR analysis. A trade-off decision therefore had to be made.

From Fig. 3 (**C**) and (**D**) we can conclude that the catalyst **C:E:M1:P2$_{80\%}$** was the more efficient one, with a productivity of 21.18 g_{prod} h^{-1} L^{-1}, compared to the other catalysts whose productivity values were substantially lower (**C:E:M1:P6$_{50\%}$** 1.43 g_{prod} h^{-1} L^{-1}; **C:E:M1:P5$_{50\%}$** 2.07 g_{prod} h^{-1} L^{-1}; **C:G:P4$_{30\%}$** 1.62 g_{prod} h^{-1} L^{-1}). **C:E:M1:P2$_{80\%}$** was stable for more than 60 h maintaining its structure (Figure S.23-S.25). Considering that all the optimisations were made with the same catalyst, the total durability was higher than 300 h. Also, when doing the reactions simulating a 2nd column or more residence time (Fig. 3 (**E**)), it was observed that the productivity reached a maximum of 27.14 g_{prod} h^{-1} L^{-1}. Therefore, a promising material for an industrial application was successfully achieved. Due to the novelty of this methodology, existing literature data regarding this reaction with epoxides is scarce. This work also presents relative advantages to the CO_2 pressure applied, which is substantially lower than the data from the literature, the same for the stability time comparable to the data, and the moderate temperature used [56–62].

The catalyst **C:E:M1:P2$_{80\%}$** stabilised around 40 % of conversion (96 % selectivity), after 10 h of activity at 6 bar and 120 ºC. This work presents advantages relatively to other works in the literature for CO_2 cycloaddition to epoxides under continuous flow, especially regarding the pressure used. Wang *et al.* [57] reported 45 % of conversion at 20 bar and 130 ºC after approximately 35 h of activity, and then it stabilized around 41 %. Sun et al. [61] reported 57.1 % of conversion at 20 bar and 90 ºC, after continuous reaction for 2 h, however the catalyst could only be used up to 24 h since stabilization was not achieved. Valverde *et al.* [58] reported 53 % of conversion after stabilization at 140 bar and 150 ºC for 10 days of continuous use. Although the conversion is important, comparing different process conditions, namely substrate concentration, flow, temperature, and catalysts, requires calculating productivity parameters, the STY. Iglesias *et al.* [6] obtained a productivity of 4.38 g_{prod}^{-1} $_{h}$ $_{L}^{-1}$ using styrene oxide and TBA·Br, a pressure of 6 bar at 100 ºC. The present work used epichlorohydrin instead, without using a co-catalyst, and achieved a substantially higher productivity of 21.18 g_{prod} h^{-1} L^{-1} at 6 bar and 120 ºC.

Ultimately, the catalyst with PIL **P2** was the most efficient. This is probably due to the increased amount of PIL present in the bead compared to the other catalysts, since there was an increment of 30 % and 50–80 % w/w concerning chitosan. As **P2** is a commercial PIL, it probably has a higher molecular weight and is more controlled than **P4**, **P5** and **P6**, which are synthesised on a small scale in the laboratory. Consequently, **P4**, **P5** and **P6** can be more easily leached during the formation of beads due to the acid-base interactions. Also, the cation moiety in **P2** is less sterically hindered, facilitating interactions with the substrate and CO_2. The fact that the catalyst with a commercial PIL was the most efficient and productive represents an economic advantage, and it is also easier to apply a material with these characteristics on an industrial scale.

Also, comparing batch with flow catalysis, it is safe to say that the flow presents several advantages, as stated in Fig. 4. After batch catalysis, the SEM and N_2 sorption results indicated that the morphology and porosity of *AEROPIL* **C:E:M1:P2$_{80\%}$** were lost. On the contrary, when used in flow, this same catalyst exhibited a smoother decrease in surface area and pore volume, while the average pore size increased, probably due to the blockage of smaller pores were, and therefore the remaining wider pores led to increase in the average pore size (a_{BET} 118 ± 6 m^2 g^{-1}; $V_{P,BJH}$ 0.66 ± 0.03 cm^3 g^{-1}; $D_{P,BJH}$ 22.2 ± 1.1 nm – Table S.9, entry 2), reinforcing the possibility of implementing this process at an industrial scale.

Based on theoretical and experimental knowledge, a mechanism can be proposed for *AEROPILs* (Figure S.26). First, mediated by the

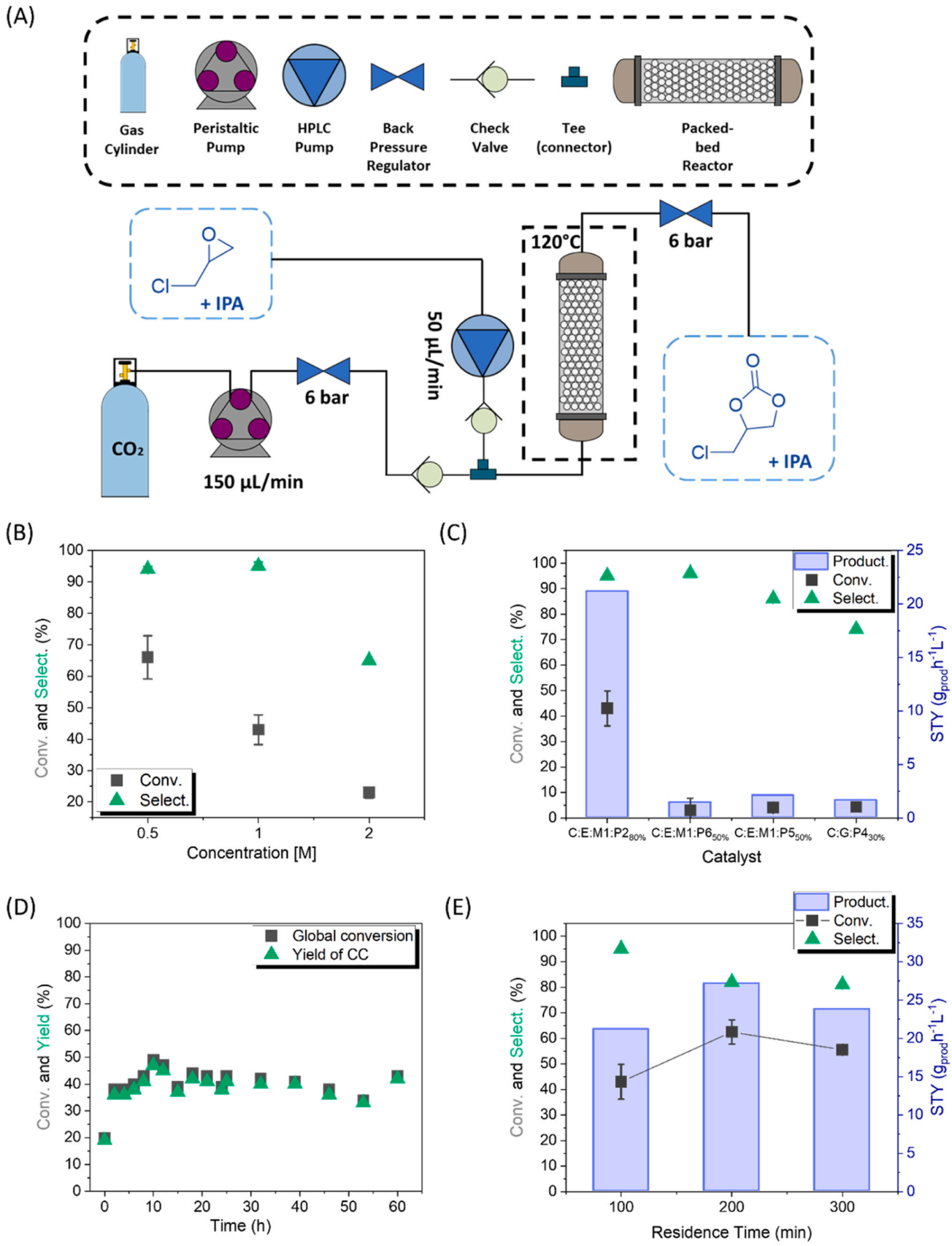

Fig. 3. **(A)** Schematic representation of continuous-flow system. **(B)** Different epichlorohydrin concentrations with the optimal reactional conditions. **(C)** Productivity of **C:E:M1:P2$_{80\%}$**, **C:E:M1:P6$_{50\%}$**, **C:E:M1:P5$_{50\%}$** and **C:G:P4$_{30\%}$**. **(D)** Stability test of **C:E:M1:P2$_{80\%}$**. **(E)** Conversion and productivity of **C:E:M1:P2$_{80\%}$** according to the residence time.

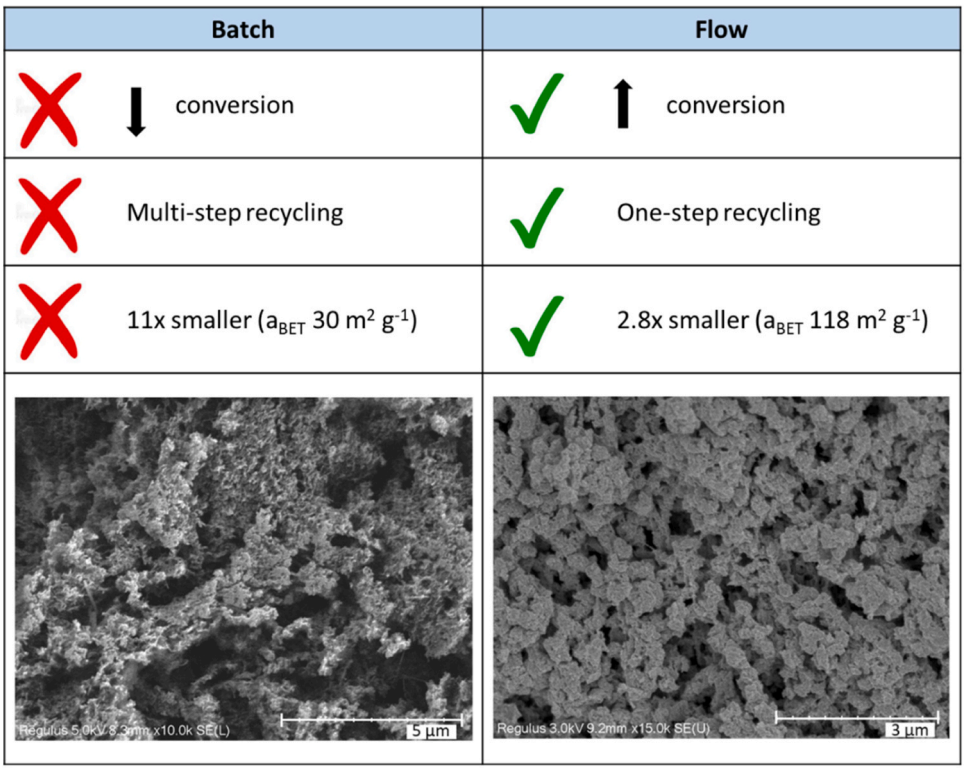

Fig. 4. Comparison between batch and continuous flow catalysis with the textural appearance of the *AEROPIL* **C:E:M1:P2$_{80\%}$** interior after catalysis by SEM imaging.

structural water contained in the *AEROPILs*, there is a hydrogen-bond donor activation between the oxygen atoms from the epoxide and -NH groups, which leads to the activation of the epoxy ring. After some time, the free halide anion, as the nucleophilic reagent, attacks the less sterically hindered carbon atom of epoxide to open the epoxy ring. The resulting oxyanion attacks a CO_2 molecule, forming an intermediate carbonate anion upon CO_2 addition. However, a competing water addition to the oxyanion can lead to a diol by-product, decreasing the reaction selectivity. When there is an intramolecular cyclisation of the oxyanion, the cyclic carbonate is formed, and the resulting free active sites can undergo the next catalytic reaction.

4. Conclusions

Efforts to combat climate change have spurred the development of new materials for efficiently capturing and converting CO_2. In this regard, PILs have shown promise as CO_2 sorbents, but challenges remain in tailoring their properties for optimal performance. Here, we report on successfully using optimized *AEROPILs* for CO_2 upcycling. *AEROPILs* with high porosity and surface area were tested as metal-free heterogeneous catalysts for CO_2 conversion in the absence of solvent and co-catalysts for the first time. We found that the combination of PILs with chitosan aerogels typically potentiates the CO_2 conversion into cyclic carbonates in a cost-effective and reusable process. Regarding batch reactions, the catalysts **C:E:M1:P2$_{80\%}$** and **C:G:P4$_{30\%}$** exhibited the highest CO_2 conversion capability with high selectivity, being that **C:E:M1:P2$_{80\%}$** remained active for 5 consecutive cycles, bringing these materials closer to the reuse that is crucial for industrial applications. Applying *AEROPILs* to continuous flow systems was explored as a stepping stone to scaling-up processes. The optimum reaction conditions were determined to be a temperature of 120 ºC, a liquid flow rate of 0.05 mL min^{-1}, and a CO_2 flow rate of 0.15 mL min^{-1}. The catalyst with the highest efficiency, **C:E:M1:P2$_{80\%}$**, exhibited a significant productivity of 21.18 g_{prod} h^{-1} L^{-1} and remained stable for over 60 h. In the end, the catalyst maintained the morphology and porosity, emphasising the advantage of implementing this process on an industrial scale.

CRediT authorship contribution statement

Raquel V. Barrulas: Writing – review & editing, Writing – original draft, Methodology, Investigation, Conceptualization. **Cristopher Tinajero:** Writing – review & editing, Software, Investigation. **Diogo P. N. Ferreira:** Writing – review & editing, Investigation. **Carlos Illanes-Bordomás:** Writing – review & editing, Investigation. **Victor Sans:** Writing – review & editing, Resources, Methodology. **Manuela Ribeiro Carrott:** Writing – review & editing, Resources, Methodology. **Carlos A. García-González:** Writing – review & editing, Resources, Methodology. **Marcileia Zanatta:** Writing – review & editing, Writing – original draft, Supervision, Project administration, Methodology, Funding acquisition, Conceptualization. **Marta C. Corvo:** Writing – review & editing, Writing – original draft, Supervision, Resources, Project administration, Methodology, Funding acquisition, Conceptualization.

Declaration of Competing Interest

The authors declare that they have no known competing financial interests or personal relationships that could have appeared to influence the work reported in this paper.

Data Availability

Data will be made available on request.

Acknowledgments

This research was funded by National Funds through FCT – Portuguese Foundation for Science and Technology, through projects LA/P/0037/2020, UIDP/50025/2020 and UIDB/50025/2020 of the Associate Laboratory Institute of Nanostructures, Nanomodelling and Nanofabrication-i3N. Also, through projects: UIDB/50006/2020, UIDP/

50006/2020, PTDC/QUI-QFI/31508/2017, PTNMR-ROTEIRO/0031/2013 and PINFRA/22161/2016, co-financed by ERDF through COMPETE 2020, PT2020, POCI and PORL and FCT through PIDDAC (POCI-01–0145-FEDER-007688, POCI-01–0145-FEDER-007265). Work supported by MICIU/AEI/10.13039/501100011033 [grant PID2020–120010RB-I00] and ERDF/EU funds. Generalitat Valenciana is gratefully acknowledged for funding for infrastructure (IDIFEDER/2021/029), GenT (CIDEGENT 2018/036) and Santiago Grisolía Programme (CIGRIS/2021/075). C.I.B. acknowledges MCINN and FSE+ for an FPI fellowship (PRE2021–097177/AEI/10.13039/501100011033). R.V.B. acknowledges FCT for the SFRH/BD/150662/2020 PhD fellowship. M.C.C. acknowledges FCT for the researcher contract (2021.03255. CEECIND). M.Z. acknowledges funding from the European Union's Horizon 2020 research and innovation programme under the Marie Skłodowska-Curie grant agreement No 101026335. R.V.B. acknowledges the COST Action CA18125 "Advanced Engineering and Research of aeroGels for Environment and Life Sciences" (AERoGELS), funded by the European Commission, for the granted Short Term Scientific Missions to perform the initial aerogels synthesis and processing in the Universidade de Santiago de Compostela, and the continuous-flow CO2 cycloadditions in the Universitat Jaume I. This work was partially supported by the project (TED2021-130288B-I00) funded by the European Union NextGenerationEU/ PRTR.

Appendix A. Supplementary data

Supporting Information**.** The supporting information is available free of charge at (…)

- Procedures for the synthesis of IL monomers and PILs, BJH-pore size distribution, nitrogen adsorption-desorption isotherm, elemental analysis, FTIR spectra, TGA curves, supporting NMR spectra, GC-MS analysis and supporting experimental data on CO_2 capture and catalysis.

Appendix A. Supporting information

Supplementary data associated with this article can be found in the online version at doi:10.1016/j.jcou.2024.102771.

References

[1] OECD/IEA, 20 Years of Carbon Capture and Storage, in: 20 Years Carbon Capture Storage, Paris, 2016. https://doi.org/10.1787/9789264267800-en.
[2] Z.J. Li, J.F. Sun, Q.Q. Xu, J.Z. Yin, Homogeneous and heterogeneous ionic liquid system: promising "ideal catalysts" for the fixation of CO2 into cyclic carbonates, ChemCatChem 13 (2021) 1848–1866, https://doi.org/10.1002/cctc.202001572.
[3] P.P. Pescarmona, Cyclic carbonates synthesised from CO2: applications, challenges and recent research trends, Curr. Opin. Green. Sustain. Chem. 29 (2021) 100457, https://doi.org/10.1016/j.cogsc.2021.100457.
[4] G.N. Bondarenko, O.G. Ganina, A.A. Lysova, V.P. Fedin, I.P. Beletskaya, Cyclic carbonates synthesis from epoxides and CO2 over NIIC-10 metal-organic frameworks, J. CO2 Util. 53 (2021) 101718, https://doi.org/10.1016/j.jcou.2021.101718.
[5] J.N. Xie, B. Yu, Z.H. Zhou, H.C. Fu, N. Wang, L.N. He, Copper(I)-based ionic liquid-catalyzed carboxylation of terminal alkynes with CO2 at atmospheric pressure, Tetrahedron Lett. 56 (2015) 7059–7062, https://doi.org/10.1016/j.tetlet.2015.11.028.
[6] D. Iglesias, C. Tinajero, S. Marchetti, I. Roppolo, M. Zanatta, V. Sans, Multi-step oxidative carboxylation of olefins with carbon dioxide by combining electrochemical and 3D-printed flow reactors, Green. Chem. (2023), https://doi.org/10.1039/D3GC03360K.
[7] J. Yuan, M. Antonietti, Poly(ionic liquid)s: Polymers expanding classical property profiles, Polym. (Guildf.) 52 (2011) 1469–1482, https://doi.org/10.1016/j.polymer.2011.01.043.
[8] S. Zulfiqar, M.I. Sarwar, D. Mecerreyes, Polymeric ionic liquids for CO2 capture and separation: potential, progress and challenges, Polym. Chem. 6 (2015) 6435–6451, https://doi.org/10.1039/C5PY00842E.
[9] W. Qian, J. Texter, F. Yan, Frontiers in poly(ionic liquid)s: syntheses and applications, Chem. Soc. Rev. 46 (2017) 1124–1159, https://doi.org/10.1039/c6cs00620e.
[10] S. Einloft, F.L. Bernard, F. Dalla Vecchia, Capturing CO2 with poly(ionic liquid)s, in: A. Eftekhari (Ed.), Polym. Ion. Liq., Royal Society of Chemistry, Cambridge, 2018, pp. 489–514.
[11] A.F. Eftaiha, A.K. Qaroush, A.K. Hasan, K.I. Assaf, F.M. Al-Qaisi, M.E. Melhem, B. A. Al-Maythalony, M. Usman, Cross-linked, porous imidazolium-based poly(ionic liquid)s for CO2 capture and utilisation, N. J. Chem. 45 (2021) 16452–16460, https://doi.org/10.1039/D1NJ02946K.
[12] X. Guo, F. Zhang, Y. Muhammad, Z. Cai, L. Gao, R. Wei, G. Xiao, Functional porous poly(ionic liquid)s catalyst for highly integrated capture and conversion of flue gas CO2, Fuel 339 (2023) 126913, https://doi.org/10.1016/j.fuel.2022.126913.
[13] G. Li, S. Dong, P. Fu, Q. Yue, Y. Zhou, J. Wang, Synthesis of porous poly(ionic liquid)s for chemical CO2 fixation with epoxides, Green. Chem. 24 (2022) 3433–3460, https://doi.org/10.1039/d2gc00324d.
[14] H. Song, Y. Wang, Y. Liu, L. Chen, B. Feng, X. Jin, Y. Zhou, T. Huang, M. Xiao, F. Huang, H. Gai, Conferring poly(ionic liquid)s with high surface areas for enhanced catalytic activity, ACS Sustain. Chem. Eng. 9 (2021) 2115–2128, https://doi.org/10.1021/acssuschemeng.0c07399.
[15] D. Jia, L. Ma, Y. Wang, W. Zhang, J. Li, Y. Zhou, J. Wang, Efficient CO2 enrichment and fixation by engineering micropores of multifunctional hypercrosslinked ionic polymers, Chem. Eng. J. 390 (2020) 124652, https://doi.org/10.1016/j.cej.2020.124652.
[16] A. Silva, R.V. Barrulas, M.C. Corvo, M. Zanatta, Tuning basic poly(ionic liquid) solutions towards atmospheric pressure CO2 capture, J. Environ. Chem. Eng. 11 (2023) 110882, https://doi.org/10.1016/j.jece.2023.110882.
[17] M. Zanatta, M. Lopes, E.J. Cabrita, C.E.S. Bernardes, M.C. Corvo, Handling CO2sorption mechanism in PIL@IL composites, J. CO2 Util. 41 (2020) 101225, https://doi.org/10.1016/j.jcou.2020.101225.
[18] R.V. Barrulas, M. Zanatta, T. Casimiro, M.C. Corvo, Advanced porous materials from poly(ionic liquid)s: Challenges, applications and opportunities, Chem. Eng. J. 411 (2021) 128528, https://doi.org/10.1016/J.CEJ.2021.128528.
[19] D. Xu, J. Guo, F. Yan, Porous ionic polymers: design, synthesis, and applications, Prog. Polym. Sci. 79 (2018) 121–143, https://doi.org/10.1016/j.progpolymsci.2017.11.005.
[20] H. Lin, S. Zhang, J. Sun, M. Antonietti, J. Yuan, Poly(ionic liquid)s with engineered nanopores for energy and environmental applications, Polym. (Guildf.) 202 (2020) 122640, https://doi.org/10.1016/j.polymer.2020.122640.
[21] R. Viveiros, S. Rebocho, T. Casimiro, Green strategies for molecularly imprinted polymer development, Polymers (Basel) 10 (2018) 1–27, https://doi.org/10.3390/polym10030306.
[22] S. Zhao, W.J. Malfait, N. Guerrero-Alburquerque, M.M. Koebel, G. Nyström, Biopolymer Aerogels and Foams: Chemistry, Properties, and Applications, Angew. Chem. - Int. Ed. 57 (2018) 7580–7608, https://doi.org/10.1002/anie.201709014.
[23] P. Latos, A. Wolny, A. Chrobok, Supported ionic liquid phase catalysts dedicated for continuous flow synthesis, Mater. (Basel) 16 (2023) 2106, https://doi.org/10.3390/ma16052106.
[24] J.A. Kozak, J. Wu, X. Su, F. Simeon, T.A. Hatton, T.F. Jamison, Bromine-catalyzed conversion of CO2 and epoxides to cyclic carbonates under continuous flow conditions, J. Am. Chem. Soc. 135 (2013) 18497–18501, https://doi.org/10.1021/ja4079094.
[25] S.G. Newman, K.F. Jensen, The role of flow in green chemistry and engineering, Green. Chem. 15 (2013) 1456, https://doi.org/10.1039/c3gc40374b.
[26] E. García-Verdugo, B. Altava, M.I. Burguete, P. Lozano, S.V. Luis, Ionic liquids and continuous flow processes: a good marriage to design sustainable processes, Green. Chem. 17 (2015) 2693–2713, https://doi.org/10.1039/C4GC02388A.
[27] F. Ferlin, D. Lanari, L. Vaccaro, Sustainable flow approaches to active pharmaceutical ingredients, Green. Chem. 22 (2020) 5937–5955, https://doi.org/10.1039/d0gc02404j.
[28] D. Valverde, R. Porcar, M. Zanatta, S. Alcalde, B. Altava, V. Sans, E. García-Verdugo, Towards highly efficient continuous-flow catalytic carbon dioxide cycloadditions with additively manufactured reactors, Green. Chem. (2022) 3300–3308, https://doi.org/10.1039/d1gc04593h.
[29] M. Garip, N. Gizli, Ionic liquid containing amine-based silica aerogels for CO2 capture by fixed bed adsorption, J. Mol. Liq. 310 (2020) 113227, https://doi.org/10.1016/j.molliq.2020.113227.
[30] X. Jiang, Y. Kong, Z. Zhao, X. Shen, Spherical amine grafted silica aerogels for CO2 capture, RSC Adv. 10 (2020) 25911–25917, https://doi.org/10.1039/d0ra04497k.
[31] S. Kumar, J. de A. e Silva, M.Y. Wani, C.M.F. Dias, A.J.F.N. Sobral, Studies of carbon dioxide capture on porous chitosan derivative, J. Dispers. Sci. Technol. 37 (2016) 155–158, https://doi.org/10.1080/01932691.2015.1035388.
[32] C. López-Iglesias, J. Barros, I. Ardao, F.J. Monteiro, C. Alvarez-Lorenzo, J. L. Gómez-Amoza, C.A. García-González, Vancomycin-loaded chitosan aerogel particles for chronic wound applications, Carbohydr. Polym. 204 (2019) 223–231, https://doi.org/10.1016/j.carbpol.2018.10.012.
[33] C. López-Iglesias, J. Barros, I. Ardao, P. Gurikov, F.J. Monteiro, I. Smirnova, C. Alvarez-Lorenzo, C.A. García-González, Jet cutting technique for the production of chitosan aerogel microparticles loaded with vancomycin, Polym. (Basel) 12 (2020) 1–13, https://doi.org/10.3390/polym12020273.
[34] C.A. García-González, T. Budtova, L. Durães, C. Erkey, P. Del Gaudio, P. Gurikov, M. Koebel, F. Liebner, M. Neagu, I. Smirnova, An opinion paper on aerogels for biomedical and environmental applications, Molecules 24 (2019) 1815, https://doi.org/10.3390/molecules24091815.
[35] N. Hsan, P.K. Dutta, S. Kumar, R. Bera, N. Das, Chitosan grafted graphene oxide aerogel: Synthesis, characterization and carbon dioxide capture study, Int. J. Biol. Macromol. 125 (2019) 300–306, https://doi.org/10.1016/j.ijbiomac.2018.12.071.

[36] N. Hsan, P.K. Dutta, S. Kumar, J. Koh, Arginine containing chitosan-graphene oxide aerogels for highly efficient carbon capture and fixation, J. CO2 Util. 59 (2022) 101958, https://doi.org/10.1016/j.jcou.2022.101958.
[37] R.V. Barrulas, C. López-Iglesias, M. Zanatta, T. Casimiro, G. Mármol, M.R. Carrott, C.A. García-González, M.C. Corvo, The AEROPILs generation: novel poly(ionic liquid)-based aerogels for CO2 capture, Int. J. Mol. Sci. 23 (2022) 200, https://doi.org/10.3390/ijms23010200.
[38] J.F. Martucci, J.P. Espinosa, R.A. Ruseckaite, Physicochemical properties of films based on bovine gelatin cross-linked with 1,4-butanediol diglycidyl ether, Food Bioprocess Technol. 8 (2015) 1645–1656, https://doi.org/10.1007/s11947-015-1524-x.
[39] W. Wan Ngah, C. Endud, R. Mayanar, Removal of copper(II) ions from aqueous solution onto chitosan and cross-linked chitosan beads, React. Funct. Polym. 50 (2002) 181–190, https://doi.org/10.1016/S1381-5148(01)00113-4.
[40] W.S.W. Ngah, S. Ab Ghani, A. Kamari, Adsorption behaviour of Fe(II) and Fe(III) ions in aqueous solution on chitosan and cross-linked chitosan beads, Bioresour. Technol. 96 (2005) 443–450, https://doi.org/10.1016/j.biortech.2004.05.022.
[41] K. AZLAN, W.N. WAN SAIME, L. LAI KEN, Chitosan and chemically modified chitosan beads for acid dyes sorption, J. Environ. Sci. 21 (2009) 296–302, https://doi.org/10.1016/S1001-0742(08)62267-6.
[42] C.A. García-González, M.C. Camino-Rey, M. Alnaief, C. Zetzl, I. Smirnova, Supercritical drying of aerogels using CO 2: Effect of extraction time on the end material textural properties, J. Supercrit. Fluids 66 (2012) 297–306, https://doi.org/10.1016/j.supflu.2012.02.026.
[43] H. Liu, A. Wang, X. Xu, M. Wang, S. Shang, S. Liu, J. Song, Porous aerogels prepared by crosslinking of cellulose with 1,4-butanediol diglycidyl ether in NaOH/urea solution, RSC Adv. 6 (2016) 42854–42862, https://doi.org/10.1039/C6RA07464B.
[44] A.S. Abdulhameed, A.H. Jawad, A.-T. Mohammad, Synthesis of chitosan-ethylene glycol diglycidyl ether/TiO2 nanoparticles for adsorption of reactive orange 16 dye using a response surface methodology approach, Bioresour. Technol. 293 (2019) 122071, https://doi.org/10.1016/j.biortech.2019.122071.
[45] Y.-Z. Du, L. Wang, Y. Dong, H. Yuan, F.-Q. Hu, Characteristics of paclitaxel-loaded chitosan oligosaccharide nanoparticles and their preparation by interfacial polyaddition in O/W miniemulsion system, Carbohydr. Polym. 79 (2010) 1034–1039, https://doi.org/10.1016/j.carbpol.2009.10.032.
[46] L. Baldino, S. Concilio, S. Cardea, I. De Marco, E. Reverchon, Complete glutaraldehyde elimination during chitosan hydrogel drying by SC-CO2 processing, J. Supercrit. Fluids 103 (2015) 70–76, https://doi.org/10.1016/j.supflu.2015.04.020.
[47] Y. He, X. Li, H. Li, J. Ding, H. Wan, G. Guan, Understanding the ingenious dual role-playing of CO2 in one-pot pressure-swing synthesis of linear carbonate, ACS Sustain. Chem. Eng. 10 (2022) 2556–2568, https://doi.org/10.1021/acssuschemeng.2c00014.
[48] A.E. Reinas, J. Hoscheid, P.M. Outuki, M.L.C. Cardoso, Preparation and characterization of microcapsules of Pterodon pubescens Benth. by using natural polymers, Braz. J. Pharm. Sci. 50 (2014) 919–930, https://doi.org/10.1590/S1984-82502014000400028.
[49] C. Ryan, E. Alcock, F. Buttimer, M. Schmidt, D. Clarke, M. Pemble, M. Bardosova, Synthesis and characterisation of cross-linked chitosan composites functionalised with silver and gold nanoparticles for antimicrobial applications, Sci. Technol. Adv. Mater. 18 (2017) 528–540, https://doi.org/10.1080/14686996.2017.1344929.
[50] A. Zając, J. Hanuza, M. Wandas, L. Dymińska, Determination of N-acetylation degree in chitosan using Raman spectroscopy, Spectrochim. Acta Part A Mol. Biomol. Spectrosc. 134 (2015) 114–120, https://doi.org/10.1016/j.saa.2014.06.071.
[51] V. Campisciano, L. Valentino, A. Morena, A. Santiago-Portillo, N. Saladino, M. Gruttadauria, C. Aprile, F. Giacalone, Carbon nanotube supported aluminum porphyrin-imidazolium bromide crosslinked copolymer: a synergistic bifunctional catalyst for CO2 conversion, J. CO2 Util. 57 (2022) 101884, https://doi.org/10.1016/j.jcou.2022.101884.
[52] Y. Zhang, D.-H. Yang, S. Qiao, B.-H. Han, Synergistic catalysis of ionic liquid-decorated covalent organic frameworks with polyoxometalates for CO 2 cycloaddition reaction under mild conditions, Langmuir 37 (2021) 10330–10339, https://doi.org/10.1021/acs.langmuir.1c01426.
[53] P. Sonzini, N. Berthet, C. Damiano, V. Dufaud, E. Gallo, A metal-free porphyrin heterogenised onto SBA-15 silica: a performant material for the CO2 cycloaddition to epoxides and aziridines, J. Catal. 414 (2022) 143–154, https://doi.org/10.1016/j.jcat.2022.08.036.
[54] Q. Yi, T. Liu, X. Wang, Y. Shan, X. Li, M. Ding, L. Shi, H. Zeng, Y. Wu, One-step multiple-site integration strategy for CO2 capture and conversion into cyclic carbonates under atmospheric and cocatalyst/metal/solvent-free conditions, Appl. Catal. B Environ. 283 (2021) 119620, https://doi.org/10.1016/j.apcatb.2020.119620.
[55] Z. Guo, X. Cai, J. Xie, X. Wang, Y. Zhou, J. Wang, Hydroxyl-exchanged nanoporous ionic copolymer toward low-temperature cycloaddition of atmospheric carbon dioxide into carbonates, ACS Appl. Mater. Interfaces 8 (2016) 12812–12821, https://doi.org/10.1021/acsami.6b02461.
[56] Y. Zhang, Z. Tan, B. Liu, D. Mao, C. Xiong, Coconut shell activated carbon tethered ionic liquids for continuous cycloaddition of CO2 to epichlorohydrin in packed bed reactor, Catal. Commun. 68 (2015) 73–76, https://doi.org/10.1016/j.catcom.2015.05.004.
[57] T. Wang, W. Wang, Y. Lyu, X. Chen, C. Li, Y. Zhang, X. Song, Y. Ding, Highly recyclable polymer supported ionic liquids as efficient heterogeneous catalysts for batch and flow conversion of CO2 to cyclic carbonates, RSC Adv. 7 (2017) 2836–2841, https://doi.org/10.1039/C6RA26780G.
[58] D. Valverde, R. Porcar, P. Lozano, E. García-Verdugo, S.V. Luis, Multifunctional Polymers Based on Ionic Liquid and Rose Bengal Fragments for the Conversion of CO2 to Carbonates, ACS Sustain. Chem. Eng. 9 (2021) 2309–2318, https://doi.org/10.1021/acssuschemeng.0c08388.
[59] M. Usman, A. Rehman, F. Saleem, A. Abbas, V.C. Eze, A. Harvey, Synthesis of cyclic carbonates from CO2 cycloaddition to bio-based epoxides and glycerol: an overview of recent development, RSC Adv. 13 (2023) 22717–22743, https://doi.org/10.1039/D3RA03028H.
[60] T. Takahashi, T. Watahiki, S. Kitazume, H. Yasuda, T. Sakakura, Synergistic hybrid catalyst for cyclic carbonate synthesis: Remarkable acceleration caused by immobilization of homogeneous catalyst on silica, Chem. Commun. (2006) 1664, https://doi.org/10.1039/b517140g.
[61] J. Sun, Z. Li, J. Yin, Continuous flow synthesis of propylene carbonate using DBU-based ionic liquid in a packed bed reactor, J. CO2 Util. 53 (2021) 101723, https://doi.org/10.1016/j.jcou.2021.101723.
[62] T.Q. Bui, L.J. Konwar, A. Samikannu, D. Nikjoo, J.-P. Mikkola, Mesoporous melamine-formaldehyde resins as efficient heterogeneous catalysts for continuous synthesis of cyclic carbonates from epoxides and gaseous CO2, ACS Sustain. Chem. Eng. 8 (2020) 12852–12869, https://doi.org/10.1021/acssuschemeng.0c03123.